CHAPTER 7

Sliding Mode Control*

Controlling the attitude dynamics of a drone is an essential task when working with aerial vehicles. This dynamics has a nonlinear nature included in the Coriolis matrix, see Chap. 2. It was demonstrated in previous chapters that generally this dynamics is used to conceive control algorithms in its linear or simplified nonlinear mode. Nevertheless, it is also possible to represent these nonlinear equations as linear and perturbed equations, implying the design of controllers in an easy way. Nonlinear controllers are becoming popular when working with UAVs because they can be robust with respect to unknown perturbations such as wind present in the environment. Several researchers have proposed countless algorithms to stabilize the attitude of the aerial vehicle. The sliding mode approach becomes an essential tool due to its robustness and quick dynamics to converge the states. This methodology has been extensively studied in many works, see [1–5].

In this chapter the sliding mode and singular optimal control methodologies are used to design nonlinear controllers to stabilize the nonlinear attitude of a quadcopter vehicle. Two results are introduced here: first, a new form to represent the nonlinear equations for the orientation of a VTOL[1] vehicle in the presence of unknown disturbances as a linear MIMO and perturbed system is presented, and second, a control law is proposed and validated in simulations and in real time to stabilize the attitude of a quadcopter.

7.1 FROM THE NONLINEAR ATTITUDE REPRESENTATION TO LINEAR MIMO EXPRESSION

The simplest form to represent the orientation of a quadcopter or VTOL vehicle is to consider two integrators in cascade with external perturbations

* This chapter was developed in collaboration with Efrain Ibarra from the Laboratoire Heudiasyc at the Université de Technologie de Compiegne in France and with M. Jimenez from the Universidad Autonoma de Nuevo Leon in Mexico.

[1] Vertical Take-Off and Landing.

Indoor Navigation Strategies for Aerial Autonomous Systems.
DOI: http://dx.doi.org/10.1016/B978-0-12-805189-4.00010-X
© 2017 Elsevier Inc. All rights reserved.

as follows:

$$\ddot{\eta} = u_\eta + w_\eta, \tag{7.1}$$

or

$$\dot{\mathbf{x}} = \bar{A}\mathbf{x} + \bar{B}_1 u_\eta + \bar{B}_2 w_\eta \quad \text{with} \quad \mathbf{x} = [\eta_1 \;\; \eta_2], \tag{7.2}$$

where η represents the attitude vector with η being ϕ, θ, or ψ, i.e., the Euler angles, roll, pitch, and yaw, respectively, u_η defines the control input, and w_η the unknown and external perturbation. Even if this representation is experimentally valid for small angles, it does not represent the Coriolis and aerodynamic effects that the aerial vehicle experiences and can generate undesirable dynamics in flight when the vehicle moves quickly.

Studying the complete nonlinear attitude equations to design the controller can be an arduous task; nevertheless, some authors prefer to consider the strongest terms in the orientation to represent their model. These equations are described in the following and, considering our experience with quadcopters, they closely represent the attitude of a quadrotor vehicle:

$$\begin{aligned}
\ddot{\phi} &= \dot{\theta}\dot{\psi}\left(\frac{I_y - I_z}{I_x}\right) - \frac{I_r}{I_x}\dot{\theta}\Omega + \frac{l}{I_x}u_\phi + w_\phi, \\
\ddot{\theta} &= \dot{\phi}\dot{\psi}\left(\frac{I_z - I_x}{I_y}\right) - \frac{I_r}{I_y}\dot{\phi}\Omega + \frac{l}{I_y}u_\theta + w_\theta, \\
\ddot{\psi} &= \dot{\theta}\dot{\phi}\left(\frac{I_x - I_y}{I_z}\right) + \frac{l}{I_z}u_\psi + w_\psi,
\end{aligned} \tag{7.3}$$

where the distance from each motor to the gravity center of the vehicle is denoted by l. The inertia of the vehicle in each axis is defined by I_x, I_y, and I_z while the inertia of the motor is represented by I_r, and the speed of the rotor is defined by Ω.

Notice that system (7.3) is quite different from (7.1) even if the unknown disturbances or uncertainties, w_η, are also considered in the model. We study the system with bounded perturbations because it is obvious that the physical characteristics of the vehicle (power motors, etc.) are not unlimited, and, as a consequence, the perturbations need to be bounded, i.e., $|w_\eta| \leqq L_\eta$, where L_η is a constant that defines the amplitude of each perturbation.

Theorem 7.1. *System (7.3) is equivalent to system*

$$\dot{\boldsymbol{x}} = A\boldsymbol{x} + B(\boldsymbol{u} + \bar{\boldsymbol{w}}) \tag{7.4}$$

with $\boldsymbol{x} = (\phi_1 \quad \theta_1 \quad \psi_1 \quad \phi_2 \quad \theta_2 \quad \psi_2)^T$, $\boldsymbol{u} = (u_\phi \quad u_\theta \quad u_\psi)^T$,

$$\bar{\boldsymbol{w}} = \begin{pmatrix} \dfrac{\theta_2\left(\psi_2\left(\dfrac{I_y - I_z}{I_x}\right) - \dfrac{I_r}{I_x}\Omega\right) - \phi_2 + w_\phi}{\dfrac{l}{I_x}} \\ \dfrac{\phi_2\left(\psi_2\left(\dfrac{I_z - I_x}{I_y}\right) - \dfrac{I_r}{I_y}\Omega\right) - \theta_2 + w_\theta}{\dfrac{l}{I_y}} \\ \dfrac{\theta_2\phi_2\left(\dfrac{I_x - I_y}{I_z}\right) - \psi_2 + w_\psi}{\dfrac{l}{I_z}} \end{pmatrix}, \quad A = \begin{pmatrix} 0_{3\times3} & \mathbb{I}_{3\times3} \\ 0_{3\times3} & \mathbb{I}_{3\times3} \end{pmatrix}, \quad B = \begin{pmatrix} 0_{3\times3} \\ B_2 \end{pmatrix},$$

$$B_2 = \begin{pmatrix} \dfrac{l}{I_x} & 0 & 0 \\ 0 & \dfrac{l}{I_y} & 0 \\ 0 & 0 & \dfrac{l}{I_z} \end{pmatrix}.$$

Proof. Consider $\gamma_1 = \left(\dfrac{I_y - I_z}{I_x}\right)$, $\gamma_2 = \left(\dfrac{I_z - I_x}{I_y}\right)$, $\gamma_3 = \left(\dfrac{I_x - I_y}{I_z}\right)$, $\beta_1 = \dfrac{I_r}{I_x}\Omega$, $\beta_2 = \dfrac{I_r}{I_y}\Omega$, $b_1 = \dfrac{l}{I_x}$, $b_2 = \dfrac{l}{I_y}$, and $b_3 = \dfrac{l}{I_z}$. Define $\phi_1 = \phi$, $\theta_1 = \theta$, $\psi_1 = \psi$, $\dot{\phi}_1 = \phi_2$, $\dot{\theta}_1 = \theta_2$, and $\dot{\psi}_1 = \psi_2$.

Then, rewriting (7.3) it follows that

$$\begin{aligned} \dot{\phi}_1 &= \phi_2, & \dot{\phi}_2 &= \theta_2(\psi_2\gamma_1 - \beta_1) + b_1 u_\phi + w_\phi, \\ \dot{\theta}_1 &= \theta_2, & \dot{\theta}_2 &= \phi_2(\psi_2\gamma_2 - \beta_2) + b_2 u_\theta + w_\theta, \\ \dot{\psi}_1 &= \psi_2, & \dot{\psi}_2 &= \theta_2\phi_2\gamma_3 + b_3 u_\psi + w_\psi. \end{aligned} \tag{7.5}$$

To simplify the analysis, define $f_1 = \theta_2(\psi_2\gamma_1 - \beta_1)$, $f_2 = \phi_2(\psi_2\gamma_2 - \beta_2)$, and $f_3 = \theta_2\phi_2\gamma_3$. Taking the three right equations of (7.5), we obtain

$$\begin{aligned} \dot{\phi}_2 &= \phi_2 - \phi_2 + f_1 + b_1 u_\phi + w_\phi, \\ \dot{\theta}_2 &= \theta_2 - \theta_2 + f_2 + b_2 u_\theta + w_\theta, \\ \dot{\psi}_2 &= \psi_2 - \psi_2 + f_3 + b_3 u_\psi + w_\psi. \end{aligned}$$

Define $\Phi_1 = f_1 - \phi_2$, $\Phi_2 = f_2 - \theta_2$, and $\Phi_3 = f_3 - \psi_2$. Then

$$\begin{aligned} \dot{\phi}_2 &= \phi_2 + b_1(u_\phi + \bar{w}_\phi), \\ \dot{\theta}_2 &= \theta_2 + b_2(u_\theta + \bar{w}_\theta), \\ \dot{\psi}_2 &= \psi_2 + b_3(u_\psi + \bar{w}_\psi) \end{aligned}$$

with $\bar{w}_i = (\Phi_i + w_\eta)/b_i$. Finally, define $\boldsymbol{\eta}_i = (\phi_i \quad \theta_i \quad \psi_i)^T$, $i = 1, 2$. Then we can write

$$\begin{aligned} \dot{\boldsymbol{\eta}}_1 &= \boldsymbol{\eta}_2, \\ \dot{\boldsymbol{\eta}}_2 &= \boldsymbol{\eta}_2 + B_2(\boldsymbol{u} + \bar{\boldsymbol{w}}), \end{aligned}$$

which is equivalent to system (7.4). □

7.2 NONLINEAR OPTIMAL CONTROLLER WITH INTEGRAL SLIDING MODE DESIGN

The goal is to stabilize the quadcopter attitude using an optimal control $\boldsymbol{u}$ that is robust with respect to perturbations and parameter variations. For this it is necessary to minimize the following singular quadratic cost:

$$J(\boldsymbol{x}(t)) = \frac{1}{2}\int_{t_1}^{\infty} \left[\boldsymbol{x}(t)^T Q \boldsymbol{x}(t)\right] dt, \tag{7.6}$$

with $Q = Q^T > 0$. The minimization of (7.6) is subject to

$$\dot{\boldsymbol{\eta}}_1 = \boldsymbol{\eta}_2. \tag{7.7}$$

Developing (7.6), it follows that

$$J = \frac{1}{2}\int_{t_1}^{\infty} \left(\boldsymbol{\eta}_1^T Q_{11} \boldsymbol{\eta}_1 + 2\boldsymbol{\eta}_1^T Q_{12} \boldsymbol{\eta}_2 + \boldsymbol{\eta}_2^T Q_{22} \boldsymbol{\eta}_2\right) dt. \tag{7.8}$$

To eliminate the cross terms, the Utkin variable $\boldsymbol{v} = \boldsymbol{\eta}_2 + Q_{22}^{-1} Q_{12}^T \boldsymbol{\eta}_1$ is used. Then

$$J = \frac{1}{2}\int_{t_1}^{\infty} (\boldsymbol{\eta}_1^T Q_1 \boldsymbol{\eta}_1 + \boldsymbol{v}^T Q_{22} \boldsymbol{v}) dt \tag{7.9}$$

with $Q_1 = Q_{11} - Q_{12} Q_{22}^{-1} Q_{12}^T$. Rewriting (7.7) with the Utkin variable yields

$$\dot{\boldsymbol{\eta}}_1 = A_1 \boldsymbol{\eta}_1 + \boldsymbol{v}, \tag{7.10}$$

where $A_1 = -Q_{22}^{-1} Q_{12}^T$. Then (7.9) is not singular with respect to the variable $\boldsymbol{v}$, so that $\boldsymbol{v}$ is taken as an optimal virtual control variable and is given by

$$\boldsymbol{v} = -Q_{22}^{-1} P \boldsymbol{\eta}_1, \tag{7.11}$$

where $P \in \mathbb{R}^{3\times 3}$ is the solution to the Riccati equation $PA_1 + A_1^T P - P\,Q_{22}^{-1} P + Q_1 = 0$. Introducing the Utkin variable into (7.11), we have

$$\eta_2 + Q_{22}^{-1}\left(Q_{12}^T + P\right)\boldsymbol{\eta_1} = \mathbf{0}. \tag{7.12}$$

Notice that (7.11) and (7.12) are only true if (7.9) is minimized for all $t_1 \geq 0$.

Observe that (7.12) is an optimal vector that can be used for designing the vector $\boldsymbol{S} \in \mathbb{R}^3$ given by

$$\boldsymbol{S} = \boldsymbol{\eta_2} + Q_{22}^{-1}\left(Q_{12}^T + P\right)\boldsymbol{\eta_1}, \tag{7.13}$$

where (7.13) represents the sliding surface vector. Taking the derivative of the previous equation with respect to time gives

$$\dot{S} = \left[\mathbb{I}_{3\times 3} + Q_{22}^{-1}\left(Q_{12}^T + P\right)\right]\boldsymbol{\eta_2} + B_2\left(\boldsymbol{u} + \bar{\boldsymbol{w}}\right). \tag{7.14}$$

To remove the linear parts, take $\boldsymbol{u}$ as

$$\boldsymbol{u} = B_2^{-1}\left\{\bar{\boldsymbol{u}} - \left[\mathbb{I}_{3\times 3} + Q_{22}^{-1}\left(Q_{12}^T + P\right)\right]\boldsymbol{\eta_2}\right\}. \tag{7.15}$$

Thus

$$\dot{S} = \bar{\boldsymbol{u}} + B_2\,\boldsymbol{w}, \tag{7.16}$$

where $\bar{\boldsymbol{u}}$ is the new controller to assure the convergence of the system. Developing the above, it follows that

$$\begin{pmatrix} \dot{S}_1 \\ \dot{S}_2 \\ \dot{S}_3 \end{pmatrix} = \begin{pmatrix} \bar{u}_1 + f_1 - \phi_2 + w_\phi \\ \bar{u}_2 + f_2 - \theta_2 + w_\theta \\ \bar{u}_3 + f_3 - \psi_2 + w_\psi \end{pmatrix}.$$

To remove the linearities $\boldsymbol{\eta_2}$, we propose $\bar{\boldsymbol{u}}$ as

$$\bar{\boldsymbol{u}} = \begin{pmatrix} \bar{u}_1 \\ \bar{u}_2 \\ \bar{u}_3 \end{pmatrix} = \begin{pmatrix} \bar{\nu}_1 + \phi_2 \\ \bar{\nu}_2 + \theta_2 \\ \bar{\nu}_3 + \psi_2 \end{pmatrix}.$$

Then, rewrite $\dot{\boldsymbol{S}}$ as

$$\dot{\boldsymbol{S}} = \begin{pmatrix} \bar{\nu}_1 + f_1 + w_\phi \\ \bar{\nu}_2 + f_2 + w_\theta \\ \bar{\nu}_3 + f_3 + w_\psi \end{pmatrix},$$

where each $\dot{S}_i \in \dot{\boldsymbol{S}}$ is represented as

$$\dot{S}_i = \bar{\nu}_i + f_i\left(\boldsymbol{\eta_1}, \boldsymbol{\eta_2}, t\right) + w_\eta. \tag{7.17}$$

7.2.1 Convergence of the Sliding Surfaces

In the conventional sliding mode control the robustness property is not guaranteed from the first time instant because the robustness is only guaranteed when the sliding surface reaches zero.

With the integral sliding mode we will be able to compensate nonlinear terms and bounded uncertainties, also the robustness will be guaranteed from the initial time instance. In the following, we introduce variable $\bar{\nu}_i$ to stabilize the sliding surfaces.

Then, we propose

$$\bar{\nu}_i = \bar{\nu}_{i1} + \bar{\nu}_{i2}. \tag{7.18}$$

- Part $\bar{\nu}_{i1}$ will be responsible of compensating the nonlinear terms f_i and the bounded disturbance w_η from the beginning.
- Component $\bar{\nu}_{i2}$ will make sure that each sliding surface S_i reaches the optimal surface $S_i = 0$ at a defined finite time t_1 taking in consideration that the perturbations f_i and w_η have been compensated from the initial time instance $t = 0$.

Design of $\bar{\nu}_{i1}$

For $\bar{\nu}_{i1}$ we propose a new auxiliary surface σ_i with $i = 1, 2, 3$ given by[2]

$$\begin{cases} \sigma_i = S_i - Z_i, \\ \dot{Z}_i = \bar{\nu}_{i\,2}. \end{cases} \tag{7.19}$$

It should be mentioned that $\bar{\nu}_{i1}$ is designed as a conventional sliding mode control. This means that for the stability analysis a candidate Lyapunov function could be used. Therefore

$$V(\sigma_i) = \frac{1}{2}\sigma_i^2 > 0. \tag{7.20}$$

The asymptotic stability of (7.19) at the equilibrium point 0 can be proved if the following conditions are satisfied:

$$\text{(a)} \lim_{|\sigma_i| \to \infty} V = \infty, \tag{7.21}$$

$$\text{(b)} \ \dot{V} < 0 \text{ for } \sigma_i \neq 0. \tag{7.22}$$

[2] In this chapter variable σ is used only as an auxiliary sliding surface and not as a saturation function.

Condition (a) is obviously satisfied by V in (7.20). Nevertheless, the finite-time convergence (global finite-time stability) could be achieved if condition (b) is modified as

$$\dot{V} \leq -\alpha_i V^{1/2}, \quad \alpha_i > 0. \tag{7.23}$$

Indeed, separating variables and integrating inequality (7.23) over the time interval $0 \leq \tau \leq t$, we obtain

$$V^{1/2}(\sigma_i(t)) \leq -\frac{1}{2}\alpha_i t + V^{1/2}(\sigma_i(0)), \tag{7.24}$$

and, considering that $V(\sigma_i(t))$ reaches zero in finite time t_r, get

$$t_r \leq \frac{2V^{1/2}(\sigma_i(0))}{\alpha_i}. \tag{7.25}$$

Therefore control $\bar{v}_{i1}$ that satisfies (7.23) will drive σ_i to zero in finite time t_r and will keep it at zero $\forall\, t \geq t_r$.

Now notice that (7.23) can be written as

$$\sigma_i \dot{\sigma}_i \leq -\bar{\alpha}_i |\sigma_i|, \qquad \bar{\alpha}_i = \frac{\alpha_i}{\sqrt{2}}, \qquad \bar{\alpha}_i > 0. \tag{7.26}$$

Consequently, from the above and with (7.17), (7.18) and (7.19) we have

$$\begin{aligned} \sigma_i * \left(\dot{S}_i - \dot{Z}_i\right) &= \sigma_i * \left(\bar{v}_{i1} + \bar{v}_{i2} + f_i\left(\boldsymbol{\eta_1}, \boldsymbol{\eta_2}, t\right) + w_\eta - \bar{v}_{i2}\right) \\ &= \sigma_i * \left(\bar{v}_{i1} + f_i\left(\boldsymbol{\eta_1}, \boldsymbol{\eta_2}, t\right) + w_\eta\right), \end{aligned}$$

and, selecting $\bar{v}_{i1} = -\rho_i \operatorname{sgn}(\sigma_i)$, condition (7.26) is fulfilled if and only if

$$\rho_i = \bar{\alpha}_i + \left|f_i\left(\boldsymbol{\eta_1}, \boldsymbol{\eta_2}, t\right)\right| + L_\eta. \tag{7.27}$$

Notice that (7.27) represents the necessary gains for ensuring the finite time stability in a bounded finite time t_r, which means

$$t_r \leq \frac{2V^{1/2}(\sigma_i(0))}{\alpha_i} = \frac{|\sigma_i(0)|}{\bar{\alpha}}. \tag{7.28}$$

The above implies that $\sigma_i = \dot{\sigma}_i = 0$ for all $t \geq t_r$, then the condition $\dot{\sigma}_i = 0$ produces

$$\dot{\sigma}_i = \underbrace{-\rho_i \operatorname{sgn}(\sigma_i)}_{\bar{v}_{i1}} + f_i\left(\boldsymbol{\eta_1}, \boldsymbol{\eta_2}, t\right) + w_\eta = 0 \quad \forall t \geq t_r,$$

meaning that $-\rho_1 \operatorname{sgn}(\sigma_i)$ will compensate the perturbative terms $f_i(\boldsymbol{\eta_1}, \boldsymbol{\eta_2}, t) + w_\eta$ only during the reaching phase.

In the following, to eliminate the reaching phase, we observe in (7.28) that proposing $\sigma_i(0) = 0$ will imply $t_r = 0$ and as a result $\sigma_i = \dot{\sigma}_i = 0$ for all $t \geq 0$.

Based on the above considerations, we present the next result

$$\bar{\nu}_{i1} = -\rho_i \operatorname{sgn}(\sigma_i) = -\left(f_i\left(\boldsymbol{\eta_1}, \boldsymbol{\eta_2}, t\right) + w_\eta\right), \quad \forall t \geq 0$$

if and only if $\sigma_i(0) = 0$.

Therefore control $\bar{\nu}_{i1} = -\rho_i \operatorname{sgn}(\sigma_i)$ compensates $f_i(\boldsymbol{\eta_1}, \boldsymbol{\eta_2}, t) + w_\eta$ for all $t \geq 0$ if and only if $\sigma_i(0) = 0$.

Now considering that control $\bar{\nu}_{i1}$ accomplishes $\sigma_i(t) = 0$ for all $t \geq 0$ and due to (7.19), it follows that $S_i(t) = Z_i(t)$ for all $t \geq 0$. Therefore (7.19) can be rewritten as

$$\begin{cases} S_i = Z_i, \\ \dot{Z}_i = \bar{\nu}_{i\,2}, \end{cases} \quad \text{with } Z_i(0) = S_i(0). \tag{7.29}$$

Then considering (7.29) we have

$$\dot{S}_i = \bar{\nu}_{i2}.$$

The next step is to design $\bar{\nu}_{i2}$ such that S_i converges to zero in finite time.

Design of $\bar{\nu}_{i2}$

In order to achieve global finite-time stability at the optimal sliding surfaces $S_i = 0$, we introduce $\bar{\nu}_{i\,2} = -k_i |S_i|^{1/2} \operatorname{sgn}(S_i)$; then $\dot{S}_i$ is written as

$$\dot{S}_i = -k_i |S_i|^{1/2} \operatorname{sgn}(S_i). \tag{7.30}$$

The following Lyapunov function is proposed to prove that (7.30) converges to zero in finite time:

$$V(S_i) = |S_i| > 0. \tag{7.31}$$

The previous equations must satisfy conditions (7.22). Observe that, by definition (7.31), condition (a) is achieved; to fulfill condition (b), we use (7.23). Notice that when introducing (7.31) into (7.23) an equivalent modified condition is obtained, which is given by

$$\frac{S_i \dot{S}_i}{|S_i|} \leq -\alpha_i |S_i|^{1/2}. \tag{7.32}$$

Introducing (7.30) into (7.32), the previous inequality becomes

$$-k_i |S_i|^{1/2} \leq -\alpha_i |S_i|^{1/2}. \tag{7.33}$$

Therefore to satisfy (7.33) each gain k_i must be equal to α_i, meaning that $k_i > 0$, and this implies that

$$\dot{V} = -\alpha_i V^{1/2} \qquad \text{if} \quad k_i = \alpha_i > 0.$$

Observe that the finite-time convergence time t_{r_i} will not be bounded, it will be exactly equal to

$$t_{r_i} = \frac{2V^{1/2}(S_i(0))}{k_i} = \frac{2|S_i(0)|^{1/2}}{k_i}; \tag{7.34}$$

consequently, $S_i = 0$ in a finite time t_{r_i}. Observe that (7.34) represents the finite-time convergence of each S_i to the optimal sliding surface $S_i = 0$. With the purpose that each S_i has the same finite time convergence, we fix $t_{r_i} = t_1 = \text{cte}$,[3] then we will be able to design the gains k_i in order to have $S_1(t_1) = S_2(t_1) = \cdots = S_n(t_1) = 0$.

Fixing $t_{r_i} = t_1 = \text{cte}$, the necessary gains for getting $S_i(t_1) = 0$ can be obtained with $k_i = \dfrac{2|S_i(0)|^{1/2}}{t_1}$.

Summarizing the methodology, it follows that when considering (7.17) and the fact that $\bar{\nu}_i = \bar{\nu}_{i1} + \bar{\nu}_{i2}$, we have

$$\dot{S}_i = \underbrace{-\rho_i \operatorname{sgn}(S_i - Z_i)}_{\bar{\nu}_{i1}} + \underbrace{\left(-k_i |S_i|^{1/2} \operatorname{sgn}(S_i)\right)}_{\bar{\nu}_{i2}} + f_i + w_\eta$$

with gains

$$\rho_i = \bar{\alpha}_i + \left|f_i\left(\boldsymbol{\eta_1}, \boldsymbol{\eta_2}, t\right)\right| + L_\eta \quad \text{and} \quad k_i = \frac{2|S_i(0)|^{1/2}}{t_1}. \tag{7.35}$$

- Component $\bar{\nu}_{i1}$ will compensate the perturbative terms $f_i(\boldsymbol{\eta_1}, \boldsymbol{\eta_2}, t) + w_\eta$ for all $t \geq 0$ if and only if $Z_i(0) = S_i(0)$.
- Considering that the perturbative terms have been compensated from the initial time, control $\bar{\nu}_{i2}$ will ensure that every S_i will converge to the optimal sliding surface $S_i = 0$ in a fixed reaching time t_1.

Therefore, component $\bar{u}_i$ from (7.15) is given by

$$\begin{aligned} \bar{u}_i &= -\rho_i \operatorname{sgn}(S_i - Z_i) - k_i |S_i|^{1/2} \operatorname{sgn}(S_i) + \eta_{2_i}, \\ Z_i &= -k_i \int |S_i|^{1/2} \operatorname{sgn}(S_i)\, dt \quad \text{with } Z_i(0) = S_i(0), \end{aligned} \tag{7.36}$$

and gains $t_1 = \text{cte}$ and $\bar{\alpha}_i = \dfrac{\alpha_i}{\sqrt{2}}$ in (7.35).

[3] cte = constant.

7.3 NUMERICAL VALIDATION

Simulations are realized to validate the proposed controllers. From section 7.1 notice that (7.3) can be expressed in regular form as

$$\begin{aligned}\dot{\boldsymbol{\eta}}_1 &= \boldsymbol{\eta}_2,\\ \dot{\boldsymbol{\eta}}_2 &= \boldsymbol{\eta}_2 + B_2(\boldsymbol{u} + \bar{\boldsymbol{w}}),\end{aligned}$$

where $\boldsymbol{\eta_1} = (\phi_1, \theta_1, \psi_1)^T$ and $\boldsymbol{\eta_2} = (\phi_2, \theta_2, \psi_2)^T$.

Following the previous control procedure, some matrices are necessary to compute $\boldsymbol{u}$. These matrices are proposed as follows:

$$Q = Q^T = \begin{pmatrix} 17 & 8 & 7 & -6 & -4 & 2 \\ 8 & 26 & 6 & 4 & 4 & 13 \\ 7 & 6 & 11 & 9 & 1 & 2 \\ -6 & 4 & 9 & 23 & 9 & 4 \\ -4 & 4 & 1 & 9 & 9 & 3 \\ 2 & 13 & 2 & 4 & 3 & 8 \end{pmatrix} > 0,$$

thus

$$Q_{11} = \begin{pmatrix} 17 & 8 & 7 \\ 8 & 26 & 6 \\ 7 & 6 & 11 \end{pmatrix},\ Q_{12} = Q_{12}^T = \begin{pmatrix} -6 & -4 & 2 \\ 4 & 4 & 13 \\ 9 & 1 & 2 \end{pmatrix},$$

$$Q_{22} = \begin{pmatrix} 23 & 9 & 4 \\ 9 & 9 & 3 \\ 4 & 3 & 8 \end{pmatrix}.$$

Therefore, from (7.9) and (7.10),

$$Q_1 = \begin{pmatrix} 13.1924 & 3.9244 & 8.0378 \\ 3.9244 & 4.5773 & 3.7113 \\ 8.0378 & 3.7113 & 6.1443 \end{pmatrix},$$

$$A_1 = \begin{pmatrix} 0.1787 & 0.1203 & -0.5601 \\ 0.4330 & -0.0034 & 0.5017 \\ -0.5017 & -1.6838 & -0.1581 \end{pmatrix}.$$

Solving the Riccati equation, it follows that

$$P = \begin{pmatrix} 25.3132 & 9.9395 & -0.5181 \\ 9.9395 & 8.9679 & -1.5217 \\ -0.5181 & -1.5217 & 4.4597 \end{pmatrix},$$

and finally $\boldsymbol{S}$ can be written as

$$\boldsymbol{S} = \boldsymbol{\eta_2} + \underbrace{Q_{22}^{-1}\left(Q_{12}^{T} + P\right)}_{M}\boldsymbol{\eta_1}, \tag{7.37}$$

where

$$M = \begin{pmatrix} M_{11} & M_{12} & M_{13} \\ M_{21} & M_{22} & M_{23} \\ M_{31} & M_{32} & M_{33} \end{pmatrix} = \begin{pmatrix} 0.9702 & -0.0036 & 0.5814 \\ -0.2404 & 1.1036 & -0.9275 \\ -0.2097 & 1.0228 & 0.8646 \end{pmatrix}.$$

Then, the sliding surfaces are given by

$$\begin{aligned} S_1 &= \phi_2 + M_{11}\phi_1 + M_{12}\theta_1 + M_{13}\psi_1, \\ S_2 &= \theta_2 + M_{21}\phi_1 + M_{22}\theta_1 + M_{23}\psi_1, \\ S_3 &= \psi_2 + M_{31}\phi_1 + M_{32}\theta_1 + M_{33}\psi_1. \end{aligned}$$

Rewriting $\boldsymbol{u} \in \mathbb{R}^3$, it follows that

$$\begin{aligned} u_\phi &= (I_x/l)\left(\bar{u}_1 - M_{13}\psi_2 - M_{12}\theta_2 - (M_{11}+1)\phi_2\right), \\ u_\theta &= (I_y/l)\left(\bar{u}_2 - M_{21}\phi_2 - M_{23}\psi_2 - (M_{22}+1)\theta_2\right), \\ u_\psi &= (I_z/l)\left(\bar{u}_3 - M_{31}\phi_2 - M_{32}\theta_2 - (M_{33}+1)\,\psi_2\right), \end{aligned}$$

with

$$\begin{aligned} \bar{u}_1 &= -\rho_1 \operatorname{sgn}(S_1 - Z_1) - k_1 |S_1|^{1/2} \operatorname{sgn}(S_1) + \phi_2, \\ Z_1 &= -k_1 \int |S_1|^{1/2} \operatorname{sgn}(S_1)\, dt \quad \text{with} \quad Z_1(0) = S_1(0), \\ \bar{u}_2 &= -\rho_2 \operatorname{sgn}(S_2 - Z_2) - k_2 |S_2|^{1/2} \operatorname{sgn}(S_2) + \theta_2, \\ Z_2 &= -k_2 \int |S_2|^{1/2} \operatorname{sgn}(S_2)\, dt \quad \text{with} \quad Z_2(0) = S_2(0), \\ \bar{u}_3 &= -\rho_3 \operatorname{sgn}(S_3 - Z_3) - k_3 |S_3|^{1/2} \operatorname{sgn}(S_3) + \psi_2, \\ Z_3 &= -k_3 \int |S_3|^{1/2} \operatorname{sgn}(S_3)\, dt \quad \text{with} \quad Z_3(0) = S_3(0), \end{aligned}$$

and gains given by

$$\begin{aligned} \rho_1 &= \left(\frac{\alpha_1}{\sqrt{2}} + |\theta_2(\psi_2\gamma_1 - \beta_1)| + L_1\right), \\ \rho_2 &= \left(\frac{\alpha_2}{\sqrt{2}} + |\phi_2(\psi_2\gamma_2 - \beta_2)| + L_2\right), \\ \rho_3 &= \left(\frac{\alpha_3}{\sqrt{2}} + |\theta_2\phi_2\gamma_3| + L_3\right). \end{aligned}$$

$$\left.\begin{aligned} k_1 &= \frac{2\,|S_1(0)|^{1/2}}{t_1} \\ k_2 &= \frac{2\,|S_2(0)|^{1/2}}{t_1} \\ k_3 &= \frac{2\,|S_3(0)|^{1/2}}{t_1} \end{aligned}\right|, \qquad t_1 = \text{cte} \tag{7.38}$$

The initial conditions were set as $\phi_1(0) = -5$, $\theta_1(0) = 2$, $\psi_1(0) = -3$, all in grad, $\phi_2(0) = 6$, $\theta_2(0) = 4$, $\psi_2(0) = 6$ in grad/s. These conditions imply $S_1(0) = -0.6026$, $S_2(0) = 10.1917$, and $S_3(0) = 6.5004$. We can also define $t_1 = 1$ s as a finite-time convergence instance for the sliding surfaces S_1, S_2, and S_3. Thus, from (7.38) we obtained $k_1 = 1.5525$, $k_2 = 6.3849$, and $k_3 = 5.0992$. Furthermore, for simulation purposes we assumed $\alpha_1 = 0.12$, $\alpha_2 = 0.14$, and $\alpha_3 = 0.2$. The bounded disturbances were selected as follows:

$$\begin{aligned} w_\phi &= 2\sin(t)\,\text{sgn}(S_1), & |w_\phi| &\leqq L_\phi = 2, \\ w_\theta &= -1.5\cos(2t)\,\text{sgn}(S_2), & |w_\theta| &\leqq L_\theta = 1.5, \\ w_\psi &= -0.5\exp(\cos(t))\,\text{sgn}(S_3), & |w_\psi| &\leqq L_\psi = 0.5\exp(1). \end{aligned}$$

The above disturbances were considered multiplied by $\text{sgn}(S_i)$ for the following reasons:

1. To observe that the effect chattering produced by $\text{sgn}(S_i)$ is not relevant for the compensation of such disturbances. We are only interested in the knowledge of the maximum amplitude that each perturbation can reach, and not in the high frequency that it can produce.
2. To graphically validate the theory. It is expected to observe an evident chattering effect in w_ϕ, w_θ, and w_ψ when $S_i = 0$ at the desired finite time $t_1 = 1$.

The following graphs were obtained when applying the proposed control scheme. From Fig. 7.1 observe that the auxiliary sliding surfaces σ_1, σ_2, and σ_3 are zero from the initial time instance, meaning that the robustness is guaranteed with respect to bounded uncertainties all the time. Besides, S_1, S_2, and S_3 converge to zero in a desired finite time $t_1 = 1$; this means that the vector of sliding surface $\boldsymbol{S} = \boldsymbol{\eta_2} + Q_{22}^{-1}(Q_{12}^T + P)\boldsymbol{\eta_1}$ converges to the optimal vector of sliding surfaces $\boldsymbol{S} = \boldsymbol{0}$ in finite time $t_1 = 1$, and with this fact every solution $\boldsymbol{\eta_1} = (\phi, \theta, \psi)^T$ and $\boldsymbol{\eta_2} = (\dot{\phi}, \dot{\theta}, \dot{\psi})^T$ that belongs to $\boldsymbol{S} = \boldsymbol{0}$ will be called an optimal sliding mode because it will be able to min-

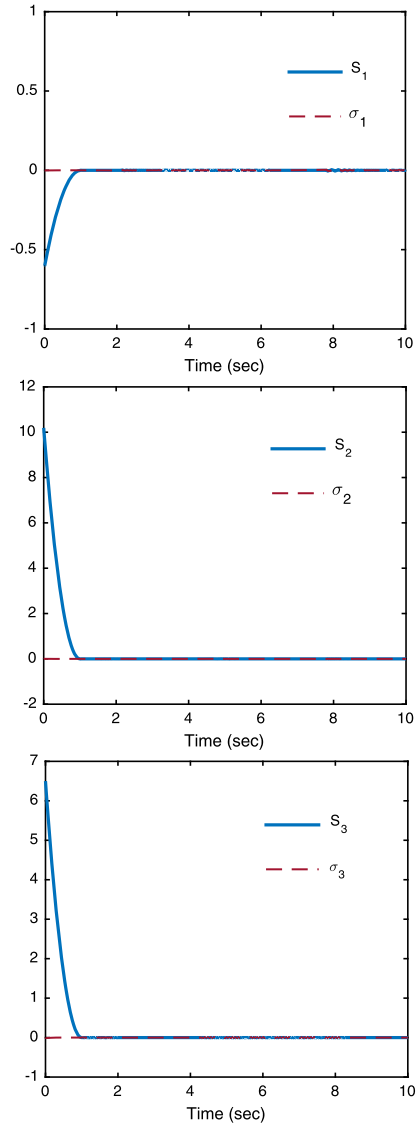

Figure 7.1 Convergence of auxiliary surfaces σ_i and sliding surfaces S_i.

imize the cost function (7.9) for all $t \geq t_1$ and in this manner solve the LQR problem.[4]

[4] This means that the state variables which minimize the quadratic cost function will be asymptotically stable.

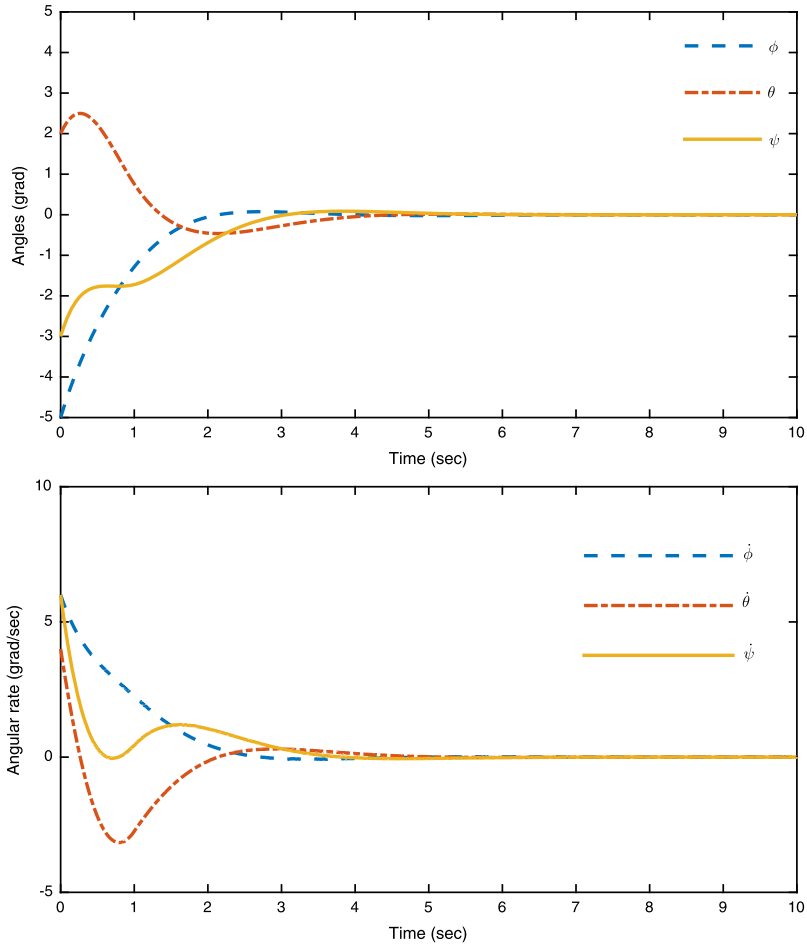

Figure 7.2 Stabilization of the dynamics of ϕ, θ, ψ and $\dot{\phi}, \dot{\theta}, \dot{\psi}$.

In Fig. 7.2 an asymptotic stabilization is clearly visible for the dynamics of ϕ, θ, ψ and $\dot{\phi}, \dot{\theta}, \dot{\psi}$ due to the convergence of the vector $\boldsymbol{S}$ to the optimal sliding vector $\boldsymbol{S} = \mathbf{0}$ in finite time $t_1 = 1$.

In Fig. 7.3 it can be observed that the bounded uncertainties w_ϕ, w_θ, and w_ψ present an evident chattering effect by considering the factor $\text{sgn}(S_i)$, and also that this chattering effect appears at time $t_1 = 1$. However, although these uncertainties present a high frequency, the control signal responses u_ϕ, u_θ, and u_ψ shown in Fig. 7.4 compensate such perturbations from the initial time instance $t = 0$.

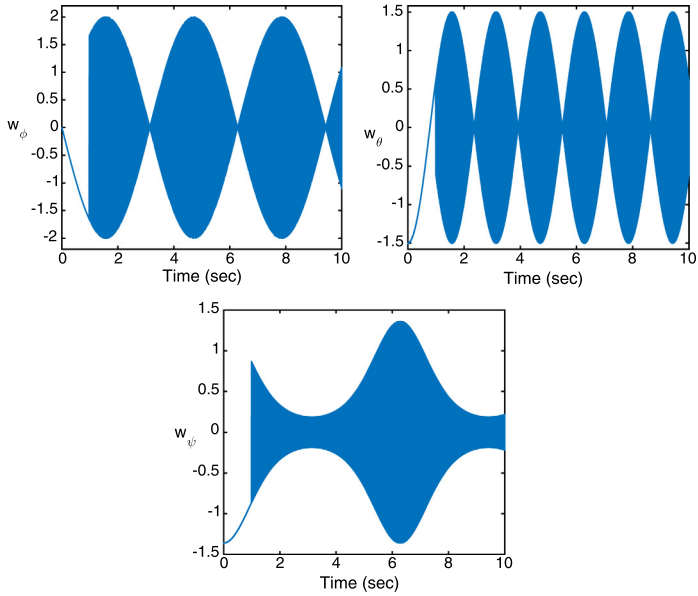

Figure 7.3 Bounded uncertainties w_ϕ, w_θ, and w_ψ.

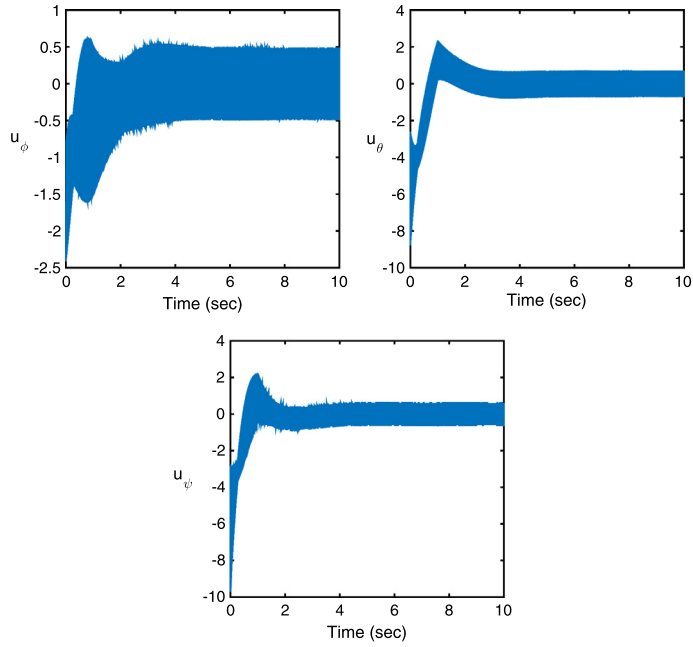

Figure 7.4 Control signals u_ϕ, u_θ, and u_ψ.

In Fig. 7.4 it is shown that the control signal responses u_ϕ, u_θ, and u_ψ have a chattering effect from the beginning, meaning that such controllers are compensating the proposed bounded uncertainties w_ϕ, w_θ, and w_ψ for all $t \geq 0$.

7.3.1 Emulation Results

One of the problems existing today is due to the discontinuity produced by the sgn function. This discontinuity produces a high frequency, normally called the chattering effect, which in practical applications is not convenient because it could produce unwanted vibrations that could damage the instruments in real-time implementations. Nevertheless, there exists extensive literature on techniques that help diminish the chattering effect.

Notice the chattering effect produced by the sgn function in Fig. 7.4. If we want to improve the performance of the control inputs, several tricks could be used. One technique used frequently is to approximate the sgn function; see, for example, [6, Chap. 1]. This approximation can be applied as

$$\text{sgn}(\sigma) \approx \frac{\sigma}{|\sigma| + \epsilon}. \tag{7.39}$$

For our simulations purposes we consider $\epsilon = 0.0007$.

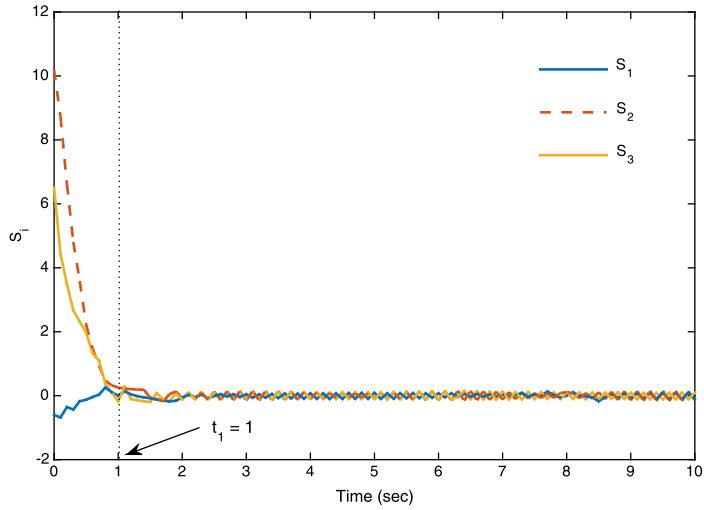

Figure 7.5 Convergence of the sliding surfaces S_1, S_2, and S_3.

The idea when validating the proposed algorithm is to have similar results in simulations and/or experiments. For this we consider that all states ϕ, θ, ψ, $\dot{\phi}$, $\dot{\theta}$, and $\dot{\psi}$ are affected by some kind of white noise (that it is true when using inertial sensors). Under these assumptions the following graphs are obtained.

In Fig. 7.5 we observe that the sliding surfaces S_1, S_2, and S_3 converge to zero in finite time t_1, although the nonlinear system is being affected by white noise. In Fig. 7.6 asymptotic convergence is observed for the dynamics of ϕ, θ, ψ and $\dot{\phi}, \dot{\theta}, \dot{\psi}$ in spite of having white noise in the internal dynamics of the system. Due to this, the controls shown in Fig. 7.7 achieve the convergence of the vector $\boldsymbol{S}$ to the optimal sliding vector $\boldsymbol{S} = \boldsymbol{0}$ in

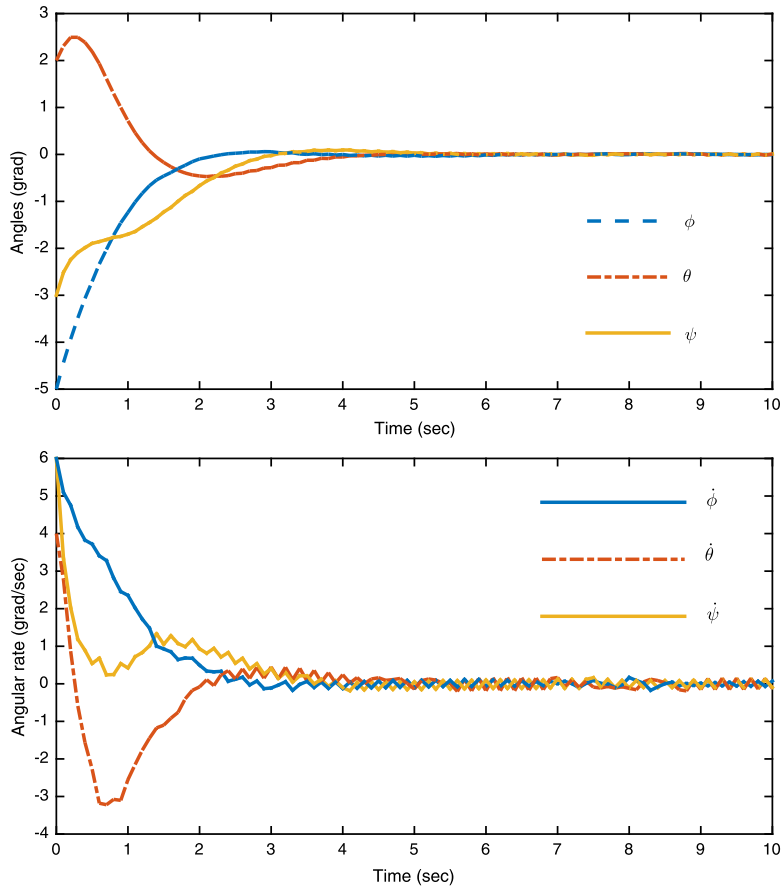

Figure 7.6 Dynamic stabilization of ϕ, θ, ψ and $\dot{\phi}, \dot{\theta}, \dot{\psi}$ with sensor noise.

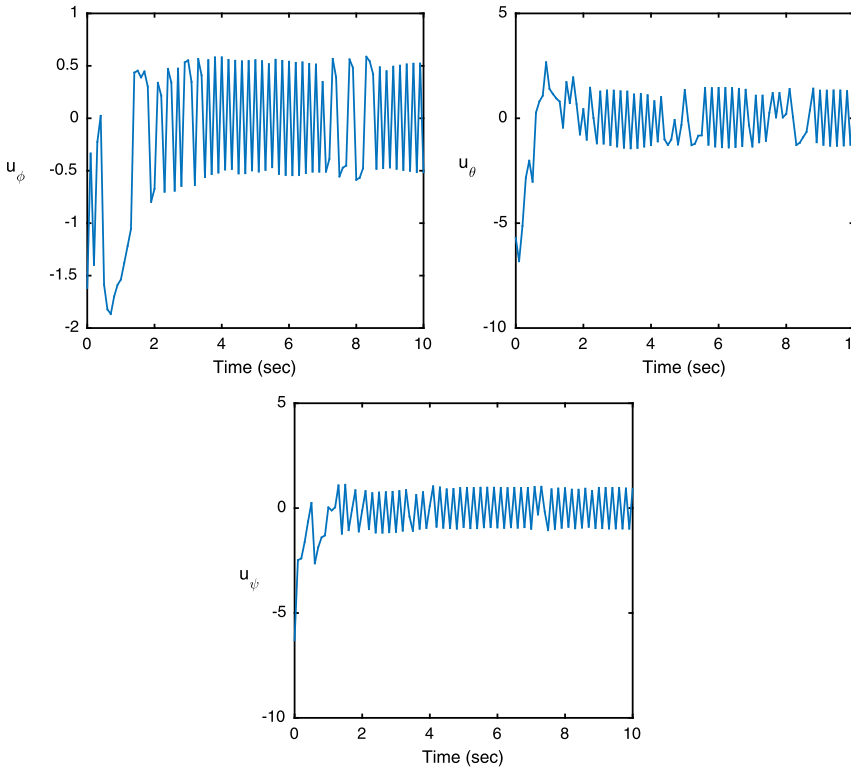

Figure 7.7 Control signals u_ϕ, u_θ, and u_ψ.

finite time. In Fig. 7.7 a representation of the controllers u_ϕ, u_θ, and u_ψ is shown; they drive $\boldsymbol{S}$ to zero in finite time in the presence of white noise and bounded uncertainties.

7.4 REAL-TIME VALIDATION

The previous controller was validated on our platform (see Sect. 4.1.5 of Chap. 4) to analyze the attitude performance of a quadcopter. Manual and aggressive references were given to test the behavior of the controller. The following main graphs illustrate the results.

Applying the controller as obtained in Sect. 7.3 in real time is very difficult, and the system is very sensible to small changes. This effect appears because even if the sliding surfaces go to zero, the cross terms of other variables are present in these surfaces, e.g., recall that surface S_1 is for assuring the roll angle convergence and notice that pitch and yaw terms are also

included. In addition, if the terms M_{ij} of these variables (pitch and yaw) are bigger then they will strongly influence the controller performance. Therefore, in this part we will include a theoretical–practical tune up that could be used for sliding controllers.

Observe that $\boldsymbol{S} = \boldsymbol{v_q} + M\boldsymbol{q}$. Then we can choose M not only to assure convergence of the sliding surfaces but also to facilitate the implementation in real time. Therefore the goal will be to weigh the main diagonal of M to assure good convergence of each state. Remember that M is given by $M = Q_{22}^{-1}\left(Q_{12}^T + P\right)$ and Q is given by

$$Q = Q^T = \begin{pmatrix} Q_{11} & Q_{12} \\ Q_{12}^T & Q_{22} \end{pmatrix} > 0, \quad Q_{11}, Q_{12}, Q_{22} \in \mathbb{R}^{3\times 3}.$$

For a practical tune up we can consider $Q_{12} = \mathbf{0_{3\times 3}}$ and Q_{22} as

$$Q_{22} = \begin{pmatrix} r & 0 & 0 \\ 0 & s & 0 \\ 0 & 0 & g \end{pmatrix}$$

with r, s, and g being positive numbers to guarantee $Q_{22} = Q_{22}^T > 0$. Hence M becomes

$$M = \begin{pmatrix} P_{11}/r & 0 & 0 \\ 0 & P_{22}/s & 0 \\ 0 & 0 & P_{33/g} \end{pmatrix} = \begin{pmatrix} M_{11} & 0 & 0 \\ 0 & M_{22} & 0 \\ 0 & 0 & M_{33} \end{pmatrix},$$

and this implies that each S_i is given by

$$\begin{aligned} S_1 &= \phi_2 + M_{11}\phi_1, \\ S_2 &= \theta_2 + M_{22}\theta_1, \\ S_3 &= \psi_2 + M_{33}\psi_1. \end{aligned}$$

Then $\boldsymbol{u} \in \mathbb{R}^3$ for practical validation is given as

$$\begin{aligned} u_\phi &= (I_x/l)\left(\bar{u}_1 - (M_{11}+1)\,\phi_2\right), \\ u_\theta &= (I_y/l)\left(\bar{u}_2 - (M_{22}+1)\theta_2\right), \\ u_\psi &= (I_z/l)\left(\bar{u}_3 - (M_{33}+1)\,\psi_2\right), \end{aligned}$$

with

$$\begin{aligned} \bar{u}_1 &= -\rho_1 \operatorname{sgn}(S_1 - Z_1) - k_1 |S_1|^{1/2} \operatorname{sgn}(S_1) + \phi_2, \\ Z_1 &= -k_1 \int |S_1|^{1/2} \operatorname{sgn}(S_1)\, dt \quad \text{with} \quad Z_1(0) = S_1(0), \\ \bar{u}_2 &= -\rho_2 \operatorname{sgn}(S_2 - Z_2) - k_2 |S_2|^{1/2} \operatorname{sgn}(S_2) + \theta_2, \end{aligned}$$

$$
\begin{aligned}
Z_2 &= -k_2 \int |S_2|^{1/2} \operatorname{sgn}(S_2)\, dt \quad \text{with} \quad Z_2(0) = S_2(0), \\
\bar{u}_3 &= -\rho_3 \operatorname{sgn}(S_3 - Z_3) - k_3 |S_3|^{1/2} \operatorname{sgn}(S_3) + \psi_2, \\
Z_3 &= -k_3 \int |S_3|^{1/2} \operatorname{sgn}(S_3)\, dt \quad \text{with} \quad Z_3(0) = S_3(0).
\end{aligned}
$$

The new gains are given by

$$
\begin{aligned}
\rho_1 &= \left(\frac{\alpha_1}{\sqrt{2}} + |\theta_2 (\psi_2 \gamma_1 - \beta_1)| + L_1 \right), \\
\rho_2 &= \left(\frac{\alpha_2}{\sqrt{2}} + |\phi_2 (\psi_2 \gamma_2 - \beta_2)| + L_2 \right), \\
\rho_3 &= \left(\frac{\alpha_3}{\sqrt{2}} + |\theta_2 \phi_2 \gamma_3| + L_3 \right),
\end{aligned}
$$

and other parameters are

$$
\left.
\begin{aligned}
k_1 &= \frac{2 |S_1(0)|^{1/2}}{t_1} \\
k_2 &= \frac{2 |S_2(0)|^{1/2}}{t_1} \\
k_3 &= \frac{2 |S_3(0)|^{1/2}}{t_1}
\end{aligned}
\right| \qquad t_1 = \text{cte},
$$

$$
\begin{aligned}
&\beta_1 = \beta_2 (\gamma_1 + 1), \qquad \gamma_3 = -\gamma_1 \left(\frac{1}{\gamma_2 (\gamma_1 + 1) + 1} \right), \\
&b_2 = \frac{b_1}{(\gamma_1 + 1)}, \qquad b_3 = \frac{b_1}{\left[\gamma_2 (\gamma_1 + 1) + 1 \right]}, \\
&b_2^{-1} = \frac{(\gamma_1 + 1)}{b_1}, \qquad b_3^{-1} = \frac{\left[\gamma_2 (\gamma_1 + 1) + 1 \right]}{b_1}.
\end{aligned}
$$

Analyzing the previous gains, we can observe that the gains for heuristic tune up are β_2, γ_1, γ_2, and b_1. Thus, the gains can be proposed as

$$
\begin{aligned}
\rho_1 &= (|\theta_2 (\psi_2 \gamma_1 - \beta_1)| + L_x), \\
\rho_2 &= \left(|\phi_2 (\psi_2 \gamma_2 - \beta_2)| + L_y \right), \\
\rho_3 &= (|\theta_2 \phi_2 \gamma_3| + L_z),
\end{aligned}
$$

and if we want $\psi_2 \gamma_1 - \beta_1 \to 0$ and $\psi_2 \gamma_2 - \beta_2 \to 0$ then for the tune up we can use the following expressions:

$$
\gamma_3 = -\frac{\gamma_1}{\gamma_1 + 1}, \quad \gamma_1, b_1 = \text{any number}, \quad b_2 = b_3 = \frac{b_1}{(\gamma_1 + 1)},
$$

and then the gains become $\rho_1 = (L_x)$, $\rho_2 = \left(L_y\right)$, and $\rho_3 = (|\theta_2 \phi_2 \gamma_3| + L_z)$.

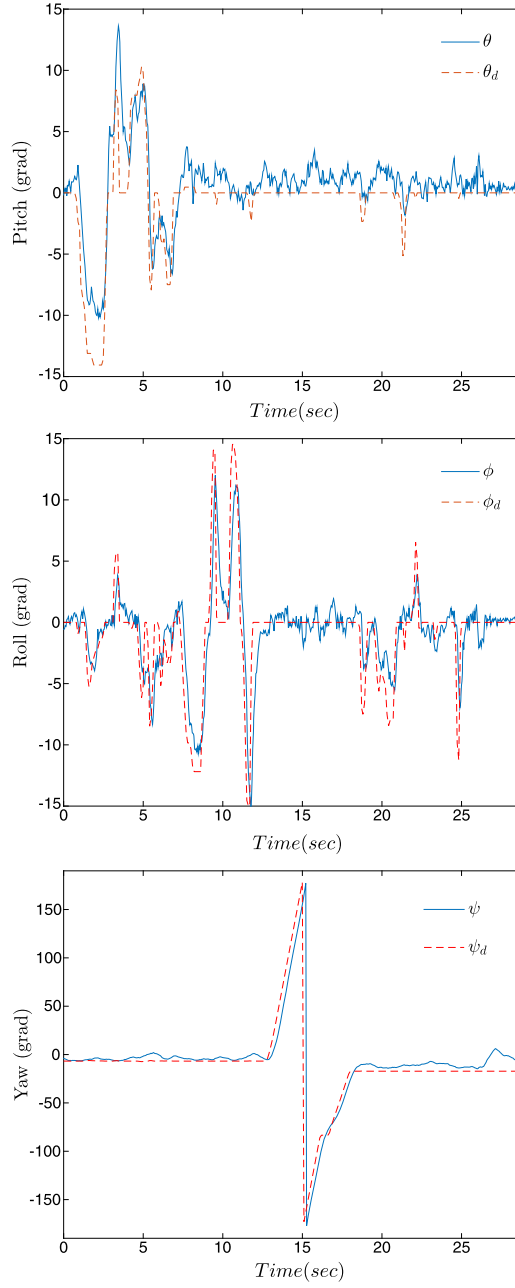

Figure 7.8 Attitude response when applying the controller in real time.

Fig. 7.8 introduces the behavior of the controllers when they are applied in a quadcopter prototype. Observe in this figure that the controller performs well in practice and that the closed-loop system is guaranteed even in the presence of aggressive maneuvers. Also notice that the procedure to tune the gains in the controller works pretty well and can be applied to others sliding controllers. Desired references were given manually by the pilot. Notice that several changes were produced to observe the performance of the controller.

7.5 DISCUSSION

Sliding mode control is becoming a popular tool when working with UAVs since robustness and quick convergence properties make such controllers very interesting to apply in autonomous vehicles. On the negative side, the main problem is the chattering effect produced in the control responses. This effect could damage the physical parts of the system and could require lots of energy for good efficiency. New controllers as proposed in this chapter try to reduce these drawbacks and improve the performance of such algorithms. Nevertheless, many issues still need to be solved and remain an open research topic.

The controller presented in this chapter was designed to be robust with respect to unknown and bounded perturbations and to guarantee convergence in finite time. This fact is not typical in controllers. From emulation results we could observe good performance of the algorithms. The next step for this controller will be to reduce the chattering effect in its design. In addition, a methodology to theoretically tune sliding algorithms was also presented in this chapter. It is very useful when applying the controller in real time. The graphs obtained when implementing the proposed controller demonstrated good performance in closed-loop system.

REFERENCES

1. T. Ledgerwood, M.E., Controllability and nonlinear control of rotational inverted pendulum, in: Advances in Robust and Nonlinear Control Systems, ASME Journal on Dynamic Systems and Control 43 (1992) 81–88.
2. A. Lukyanov, Optimal nonlinear block-control method, in: Proceedings of the 2nd European Control Conference, Groningen, Netherlands, 1993, pp. 1853–1855.
3. A. Lukyanov, S.J. Dodds, Sliding mode block control of uncertain nonlinear plants, in: Proceedings of the IFAC World Congress, San Francisco, CA, USA, 1996, pp. 241–246.
4. V. Utkin, Sliding Modes in Control and Optimization, Springer-Verlag, 1992.

5. V. Utkin, J. Guldner, J. Shi, Sliding Mode Control in Electromechanical Systems, Taylor and Francis, 1999.
6. Y. Shtessel, C. Edwards, L. Fridman, A. Levant, Sliding Mode Control and Observation, Birkhäuser, 2014.